Low-Rank Modeling of Local k-Space Neighborhoods: From Phase and Support Constraints to Structured Sparsity

Justin P. Haldar

Department of Electrical Engineering, University of Southern California, Los Angeles, CA

ABSTRACT

Low-rank modeling of local k-space neighborhoods (LORAKS) is a recent novel framework for constrained MRI reconstruction. LORAKS relies on embedding MRI data into carefully-constructed matrices, which will have low-rank structure when the MRI image has sparse support or slowly-varying phase. Low-rank matrix representation allows MRI images to be reconstructed from undersampled data using modern low-rank matrix techniques, and enables data acquisition strategies that are incompatible with more traditional representations. This paper reviews LORAKS, and describes extensions that allow LORAKS to additionally impose structured transform-domain sparsity constraints (e.g., structured sparsity of the image derivatives or wavelet coefficients).

Keywords: Low-Rank Matrix Completion, Constrained MRI Reconstruction, Structured Sparsity

1. INTRODUCTION

Magnetic resonance imaging (MRI) is a powerful technology that enables detailed and noninvasive exploration of the anatomy, structure, function, and biochemistry of living subjects. These capabilities have revolutionized modern biomedical research and clinical practice, and given rise to a multi-billion dollar global MRI industry. However, MRI data acquisition is also relatively slow, and the ability to make MRI faster has been a primary goal for the MRI community since the technology was introduced in the early 1970s. A longstanding approach to achieving faster MRI has been to sample the data below the Nyquist rate, using prior knowledge and various constraints to ensure that the image reconstruction inverse problem remains well-posed.[1]

Some of the earliest constrained MRI approaches leveraged the prior information that many MRI images will have limited spatial[2] or spatial-spectral support;[3–5] slowly-varying spatial image phase;[6–8] piecewise constant, piecewise polynomial, or piecewise smooth structure[9–12] (i.e., equivalent to assuming signal sparsity after applying differential operators or wavelet transforms); or linearly-predictable Fourier transforms.[13–16] In recent years, there has been a resurgence of interest in such constraints, spurred by the emergence of "compressed sensing" theory for recovering sparse vectors and low-rank matrices from limited measurements.[17–19] While the performance guarantees arising from compressed sensing theory are rarely applicable to practical MRI problems,[20] recent compressed sensing work has yielded novel problem formulations, data acquisition schemes, and algorithms that have substantially enhanced the flexibility and utility of constrained MRI reconstruction methods.[20–29]

In this paper, we review and generalize low-rank modeling of local k-space neighborhoods (LORAKS),[28–33] which is a novel framework that our group has been developing over the past several years. The LORAKS framework can be viewed as a combination of classical MRI assumptions with more recent compressive sensing ideas. Specifically, our previous LORAKS work[28] demonstrated that MRI images that obey support and phase constraints can be mapped into higher-dimensional structured low-rank matrices. While support and phase constraints are classical in MRI,[2–8] the existing methods generally required precise prior knowledge of the image support and/or phase, and calibrating this prior information generally required measuring extra MRI data. A unique feature of LORAKS is that the low-rank formulation allows the use of support and phase constraints without requiring calibration or detailed prior information about the image support and phase. Instead, the Fourier-domain linear prediction (subspace) relationships that are inherent to images with limited support and/or slowly-varying phase can be indirectly inferred from the undersampled data. As will be shown, LORAKS modeling also provides an easy new way to impose structured (regional) sparsity constraints. In addition,

Further author information: E-mail: jhaldar@usc.edu, Telephone: 1 213 740 2358

Wavelets and Sparsity XVI, edited by Manos Papadakis, Vivek K. Goyal, Dimitri Van De Ville,
Proc. of SPIE Vol. 9597, 959710 · © 2015 SPIE · CCC code: 0277-786X/15/$18
doi: 10.1117/12.2186705

Downloaded From: http://proceedings.spiedigitallibrary.org/ on 11/21/2016 Terms of Use: http://spiedigitallibrary.org/ss/termsofuse.aspx

LORAKS enables novel sampling schemes that are incompatible with existing reconstruction methods (including popular sparsity-based reconstructions).

In the present paper, we will also extend the LORAKS framework to incorporate constraints that are appropriate for images that approximately have piecewise polynomial or structured wavelet representations, based on theoretical insights from earlier imaging literature.[11,34] For example, Liang *et al.* demonstrated more than 25 years ago that piecewise polynomial images will satisfy special linear prediction relationships that can be inferred from a Nyquist-sampled region of measured data by embedding the data into a low-rank matrix.[11] In this paper, this idea is generalized using the LORAKS framework to indirectly infer and enforce these same linear prediction relationships from undersampled data.

During the preparation of this work, related methods by other groups emerged[35–37] that make similar LORAKS generalizations for piecewise-polynomial images that were motivated by the finite rate of innovation (FRI) signal modeling and reconstruction framework.[38*] Since these methods were developed independently, there are many theoretical and implementation differences between our work and the recent work by other groups, and we believe that each provides distinct and complementary perspectives. For example, these other approaches[35–37] are also formulated based on transform-domain sparsity, but unlike transform-domain LORAKS, they make strong assumptions that the transform coefficients are only non-zero on a set of measure zero, and do not emphasize the need for the transform domain coefficients to possess structured zeros. While these strong assumptions enable explicit theoretical performance guarantees[35–37,39] that are not available for LORAKS, the theory for these methods does not provide explicit insights into the behavior of low-rank matrix models for realistic MR images where strong support assumptions are likely to be violated. In contrast, our LORAKS-based perspective allows us to describe the effects of low-rank matrix approximation on general images as viewed from general transform domains, and these results suggest that low-rank matrix completion approaches can be successful for a broad class of signals that do not fit the modeling assumptions used by the related methods.[35–37]

2. BACKGROUND AND NOTATION

In the following, we will denote the unknown complex MR image by $\rho(\mathbf{x})$, where $\mathbf{x} \in \mathbb{R}^D$ denotes spatial location.[†] We will assume that $\rho(\mathbf{x})$ belongs to the Lebesgue space $\mathcal{L}_2(\mathbb{R}^D)$ and is finitely-supported in the spatial domain. For simplicity, we will assume that $\mathbf{x}$ has been normalized such that $\rho(\mathbf{x}) = 0$ whenever $\|\mathbf{x}\|_{\ell_\infty} > \frac{1}{2}$, where $\|\cdot\|_{\ell_p}$ denotes the standard ℓ_p-norm for finite-dimensional vectors.

We will define the *field of view* (FOV) as the set of spatial locations $\Gamma \triangleq \{\mathbf{x} \in \mathbb{R}^D : \|\mathbf{x}\|_{\ell_\infty} \leq \frac{1}{2}\}$, and define the *spatial support* of the image as the set of spatial locations $\Omega \triangleq \{\mathbf{x} \in \mathbb{R}^D : \rho(\mathbf{x}) \neq 0\}$. Note that the spatial support is a subset of the FOV. We will define the *complement of the spatial support* as the set $\Upsilon \triangleq \{\mathbf{x} \in \Gamma : \rho(\mathbf{x}) = 0\}$. Note that Ω and Υ are disjoint sets, whose union equals the FOV (i.e., $\Gamma = \Omega \bigcup \Upsilon$).

We also assume that $\rho(\mathbf{x})$ can be decomposed into magnitude $m(\mathbf{x})$ and phase $\phi(\mathbf{x})$ terms such that $\rho(\mathbf{x}) = m(\mathbf{x})e^{i\phi(\mathbf{x})}$. Note that $e^{i\phi(\mathbf{x})}$ is uniquely determined for $\mathbf{x} \in \Omega$, but the phase can be arbitrarily defined for $\mathbf{x} \in \Upsilon$.

In its simplest variations, MRI is accurately modeled as a Fourier imaging modality. We will use $\tilde{\rho}(\mathbf{k})$ to denote the Fourier transform of $\rho(\mathbf{x})$ (the so-called "k-space" signal), with

$$\tilde{\rho}(\mathbf{k}) \triangleq \int_{\mathbf{x}\in\Gamma} \rho(\mathbf{x}) e^{-i2\pi\mathbf{k}^T\mathbf{x}} d\mathbf{x} \text{ for } \mathbf{k} \in \mathbb{R}^D. \tag{1}$$

Since $\rho(\mathbf{x})$ is finitely-supported, it is sufficient to consider the Nyquist-sampled version of $\tilde{\rho}(\mathbf{k})$, which we denote by $\tilde{\rho}[\mathbf{n}]$ with $\mathbf{n} \in \mathbb{Z}^D$. Due to our normalization of $\mathbf{x}$, the Nyquist interval corresponding to Γ is unity along each spatial dimension, which yields

$$\tilde{\rho}[\mathbf{n}] \triangleq \int_{\mathbf{x}\in\Gamma} \rho(\mathbf{x}) e^{-i2\pi\mathbf{n}^T\mathbf{x}} d\mathbf{x} \text{ for } \mathbf{n} \in \mathbb{Z}^D. \tag{2}$$

[*]Note that the work by Liang *et al.*[11] can be viewed a special case of the FRI framework, though was published much earlier than the recent popularization of FRI within the signal processing community.[38]

[†]In higher dimensional imaging scenarios, $\mathbf{x}$ may represent more than just spatial variables and, e.g., could include a combination of spatial, temporal, or experimental contrast variables.

Downloaded From: http://proceedings.spiedigitallibrary.org/ on 11/21/2016 Terms of Use: http://spiedigitallibrary.org/ss/termsofuse.aspx

The data acquisition procedure for a simple single-channel Cartesian MRI experiment can be modeled as

$$\mathbf{d}_m = \tilde{\rho}[\mathbf{n}_m] + \mathbf{w}_m \text{ for } m = 1, 2, \ldots, M, \tag{3}$$

where $\mathbf{d}_m \in \mathbb{C}$ is the mth measured data sample, $\mathbf{n}_m \in \mathbb{R}^D$ is the corresponding k-space location for that sample, $\mathbf{w}_m \in \mathbb{C}$ is a noise sample, and M is the total number of measured samples. We will use $\mathbf{d} \in \mathbb{C}^M$ and $\mathbf{w} \in \mathbb{C}^M$ to denote the vectors obtained by concatenating the individual $\mathbf{d}_m$ and $\mathbf{w}_m$ values, respectively. The statistics of $\mathbf{w}$ are accurately modeled using a zero-mean circular complex white Gaussian noise distribution.

While $\tilde{\rho}[\mathbf{n}]$ is infinite dimensional, MRI experiment duration is proportional to the number of measured samples M, so $\tilde{\rho}[\mathbf{n}]$ is never sampled infinitely. Instead, it is typical to only measure from a finite region of k-space defined by $\Xi \triangleq \{\mathbf{n} \in \mathbb{Z}^D : \|\mathbf{n}\|_{\ell_\infty} \leq K\}$. The choice of K in the definition of Ξ determines the amount of Fourier truncation, and therefore the nominal spatial resolution of the experiment. We use the symbol $\tilde{\boldsymbol{\rho}}$ to denote the vector formed by concatenating the values of the ideal fully-sampled Fourier data $\tilde{\rho}[\mathbf{n}]$ for $\mathbf{n} \in \Xi$.

For accelerated imaging, it is standard to substantially subsample Ξ. Using the matrix $\mathbf{U}$ to denote this subsampling operation (formed by removing rows from an identity matrix), MRI acquisition can be modeled as

$$\mathbf{d} = \mathbf{U}\tilde{\boldsymbol{\rho}} + \mathbf{w}. \tag{4}$$

The goal of constrained MRI reconstruction is to estimate $\tilde{\boldsymbol{\rho}}$ from measurements $\mathbf{d}$. This is an ill-posed under-determined problem, and additional constraints are required to obtain a unique and stable solution.

3. REVIEW OF LORAKS

3.1 Support Constraints and the C-Matrix

Support-constrained LORAKS[28] was derived based on an assumption that the image support Ω is smaller than the FOV Γ, or equivalently, that the complement of the support Υ is a measurable (non-empty) set. In this case, it is clear that for any non-zero function $f(\mathbf{x}) \in \mathcal{L}_2(\mathbb{R}^D)$ that is supported on Υ, we must have that

$$\rho(\mathbf{x})f(\mathbf{x}) = 0 \text{ for } \forall \mathbf{x} \in \mathbb{R}^D. \tag{5}$$

By invoking the convolution property of the Fourier transform, it is straightforward to derive that

$$\sum_{\mathbf{m} \in \mathbb{Z}^D} \tilde{\rho}[\mathbf{n} - \mathbf{m}]\tilde{f}[\mathbf{m}] = 0 \text{ for } \forall \mathbf{n} \in \mathbb{Z}^D, \tag{6}$$

where $\tilde{f}[\mathbf{n}]$ is the Nyquist-sampled Fourier transform of $f(\mathbf{x})$. Importantly, Eq. (6) indicates that the k-space samples $\tilde{\rho}[\mathbf{n}]$ are linearly independent, and that a missing sample can be recovered through a weighted linear combination of the remaining samples.[34] From a different but related perspective,[38] the k-space data of images supported on Ω will have a finite rate of innovation, and $\tilde{f}[\mathbf{n}]$ will be a corresponding "annihilating filter." Since there will generally be many linearly independent functions $f(\mathbf{x}) \in \mathcal{L}_2(\mathbb{R}^D)$ that are supported on Υ, there will also generally be multiple linearly independent Fourier-domain annihilating filters.

Classical MRI reconstruction methods that use support constraints assume that Ω and/or $\tilde{f}[\mathbf{m}]$ are given as prior information.[2–5,34] However, knowledge of Ω and $\tilde{f}[\mathbf{m}]$ generally requires a calibration procedure that involves additional MRI data acquisition and prolongs the MRI experiment. A novel observation of LORAKS is that Eq. (6) implies that the fully-sampled k-space data $\tilde{\rho}[\mathbf{n}]$ can be rearranged into an approximately low-rank matrix $\mathbf{C}$, and low-rank matrix recovery techniques[19] can be used to recover missing information if $\tilde{\rho}[\mathbf{n}]$ is not fully acquired. Importantly, this procedure does not require prior knowledge of Ω.

Construction of the $\mathbf{C}$ matrix is based on the assumption that $f(\mathbf{x})$ is a smooth-enough function that it is approximately bandlimited. Specifically, we assume that $\tilde{f}[\mathbf{m}] \approx 0$ whenever $\|\mathbf{m}\|_{\ell_2} > R$, where the user-defined neighborhood radius parameter R defines the bandwidth of $\tilde{f}[\mathbf{m}]$. Letting $\Lambda = \{\mathbf{m} \in \mathbb{Z}^D : \|\mathbf{m}\|_{\ell_2} \leq R\}$ and using $|\Lambda|$ to denote the cardinality of Λ, this approximation allows Eq. (6) to be rewritten as

$$\sum_{\mathbf{m} \in \Lambda} \tilde{\rho}[\mathbf{n} - \mathbf{m}]\tilde{f}[\mathbf{m}] \approx 0 \text{ for } \forall \mathbf{n} \in \mathbb{Z}^D. \tag{7}$$

Downloaded From: http://proceedings.spiedigitallibrary.org/ on 11/21/2016 Terms of Use: http://spiedigitallibrary.org/ss/termsofuse.aspx

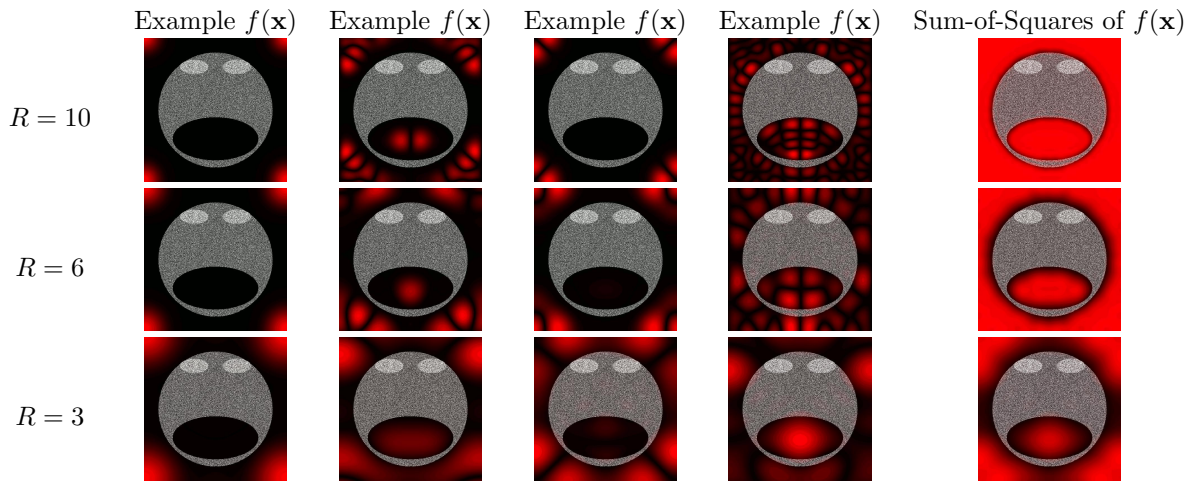

Figure 1: Illustration of the support information that can be extracted from the $\mathbf{C}$ matrix. For each subfigure, the grayscale image depicts a simulated support-limited MR image $\rho(\mathbf{x})$. The images on the left show the magnitudes of different $f(\mathbf{x})$ functions (overlaid in red) computed from the right singular vectors of the $\mathbf{C}$ matrix associated with small singular values. The red overlays in the images on the right show the sum-of-squares of $f(\mathbf{x})$ functions corresponding to small singular values. Notice that the red sum-of-squares signal clearly delineates the complement of the image support, demonstrating that the support information is embedded the subspace structure of $\mathbf{C}$. Results are shown for different values of the neighborhood radius R, which controls the bandwidth of the $f(\mathbf{x})$ functions. Larger values of R allow more precise delineation of the image support, though this comes at the expense of larger $\mathbf{C}$ matrices with increasing matrix rank.

The matrix $\mathbf{C}$ is then formed by evaluating Eq. (7) on a finite set of $\mathbf{n}$ values $\{\mathbf{n}_q\}_{q=1}^{Q}$, and then representing the resulting system of equations in matrix-vector form as:

$$\mathbf{C}\tilde{\mathbf{f}} \approx \mathbf{0}, \tag{8}$$

where $\tilde{\mathbf{f}} \in \mathbb{C}^{|\Lambda|}$ is the vector of $\tilde{f}[\mathbf{m}_\ell]$ values (where we have assumed an indexing for the elements of Λ such that $\Lambda = \{\mathbf{m}_\ell\}_{\ell=1}^{|\Lambda|}$), and $\mathbf{C} \in \mathbb{C}^{Q\times|\Lambda|}$ is a Toeplitz-like convolution matrix that has entries

$$\mathbf{C}_{q\ell} = \tilde{\rho}[\mathbf{n}_q - \mathbf{m}_\ell] \text{ for } q = 1, \ldots, Q \text{ and } \ell = 1, \ldots |\Lambda|. \tag{9}$$

Clearly, the $\mathbf{f}$ vectors correspond to the approximate nullspace vectors of the $\mathbf{C}$ matrix (i.e., the right singular vectors associated with the smallest singular values)[‡], and the $\mathbf{C}$ matrix will have low-rank. And interestingly, the nullspace vectors can be inverse Fourier transformed to find corresponding $f(\mathbf{x})$ functions that identify the support of the image $\rho(\mathbf{x})$. This is illustrated in Fig. 1. In addition, the subspace structure of the $\mathbf{C}$ matrix encodes information about the spatial distribution of signal energy for $\rho(\mathbf{x})$, even if $\rho(\mathbf{x})$ does not have strictly limited support. As a result, low-rank approximation of the $\mathbf{C}$ matrix has the effect of setting the smallest-intensity regions of $\rho(\mathbf{x})$ equal to zero. This is illustrated in Fig. 2.

As can be seen, sparse approximation using the $\mathbf{C}$ matrix is similar to more conventional sparse approximation of vectors. However, an important difference is that low-rank matrix approximation enforces structured sparsity: instead of setting isolated coefficients equal to zero as in standard sparse approximation, low-rank matrix approximation sets connected regions of the image equal to zero, with the size of these regions controlled by the parameter R. As a result of this, low-rank modeling of the $\mathbf{C}$ matrix can be more powerful than conventional sparse modeling, particularly for scenarios when the image support has compact structure. Another substantial difference between support modeling through the $\mathbf{C}$ matrix and conventional sparse modeling is that

[‡]It should be noted that the nullspaces of similarly-constructed matrices have also been important in previous applications like blind deconvolution.[40–42] While the nullspace structures are different for the different application contexts, the similarities are no coincidence. Due to space constraints, we will not elaborate further.

Downloaded From: http://proceedings.spiedigitallibrary.org/ on 11/21/2016 Terms of Use: http://spiedigitallibrary.org/ss/termsofuse.aspx

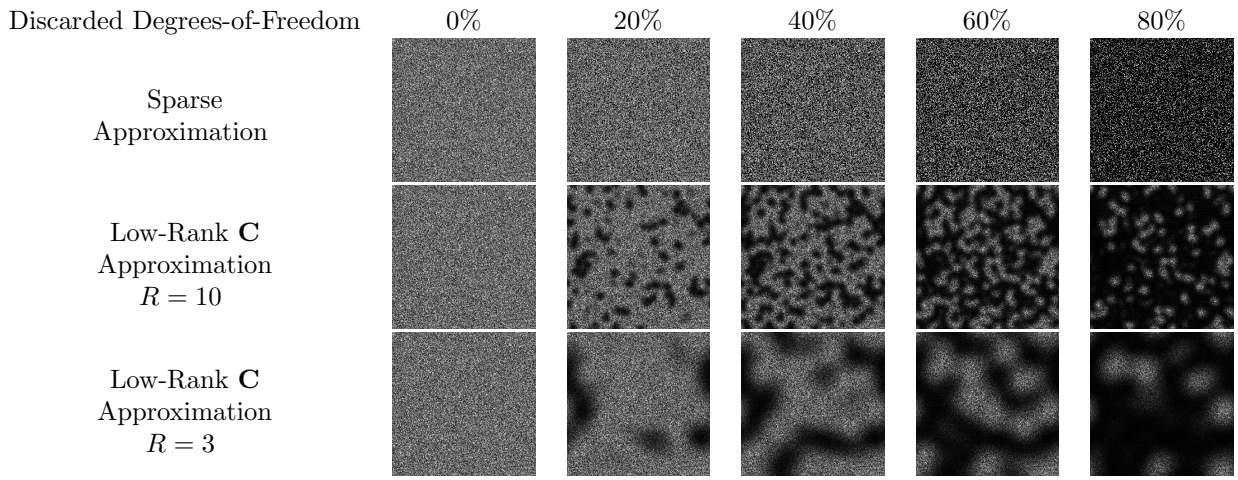

Figure 2: Comparison of sparse approximation versus **C**-based low-rank approximation for an image that does not have limited spatial support. The first row of images shows the results of spatial-domain sparse approximation of a random Gaussian image. In this case, the smallest-intensity voxels are set to zero first, regardless of the spatial context. The bottom two rows show the results of low-rank approximation of the **C** matrix. As can be seen, low-rank approximation imposes a form of structured (regional) sparsity in the image domain, with regions with the smallest signal energy being set to zero first. The region size depends on the neighborhood radius R.

the **C** matrix formulation does not require discretization of $\rho(\mathbf{x})$ in the image domain. Instead, sparse support constraints are imposed in an "off-the-grid" manner, which is beneficial because discretization is a well-known practical source of error for sparsity-constrained inverse problems.[43]

3.2 Phase Constraints and the S-Matrix

Phase-constrained LORAKS[28,30] was derived based on the well-known conjugate symmetry property of the Fourier transform that would be observed if $\rho(\mathbf{x})$ were a real-valued image.[§] While $\rho(\mathbf{x})$ is not real-valued in MRI, the corresponding magnitude image $m(\mathbf{x})$ will be. In addition, we have the relationships that

$$m(\mathbf{x})e^{-i2\pi\mathbf{q}^T\mathbf{x}} = \rho(\mathbf{x})e^{-i\phi(\mathbf{x})}e^{-i2\pi\mathbf{q}^T\mathbf{x}} = \rho^*(\mathbf{x})e^{i\phi(\mathbf{x})}e^{-i2\pi\mathbf{q}^T\mathbf{x}} \text{ for } \forall\mathbf{q}\in\mathbb{Z}^D, \tag{10}$$

where $\rho^*(\mathbf{x})$ is the complex conjugate of $\rho(\mathbf{x})$ and $\mathbf{q}\in\mathbb{Z}^D$ can be arbitrarily chosen. If we assume that the image phase is smoothly-varying such that $e^{-i\phi(\mathbf{x})}e^{-i2\pi\mathbf{q}^T\mathbf{x}}$ is approximately bandlimited to the set Λ of radius R, and if we use $\tilde{h}[\mathbf{n}]$ to denote the sampled Fourier transform of $e^{-i\phi(\mathbf{x})}$, Eq. (10) can be represented in the Nyquist-sampled Fourier domain as

$$\sum_{\mathbf{m}\in\Lambda}\tilde{\rho}[\mathbf{n}-\mathbf{m}]\tilde{h}[\mathbf{m}+\mathbf{q}] - \tilde{\rho}^*[-\mathbf{n}-\mathbf{m}]\tilde{h}^*[\mathbf{m}-\mathbf{q}] = 0 \text{ for } \forall\mathbf{n}\in\mathbb{Z}^D \text{ and } \forall\mathbf{q}\in\mathbb{Z}^D, \tag{11}$$

where $\tilde{h}^*[\mathbf{n}]$ is the complex conjugate of $\tilde{h}[\mathbf{n}]$. It should be noted that Eq. (11) has similar convolution structure to Eq. (7), which was used to construct the **C** matrix. However, there are also some important differences. Specifically, Eq. (11) involves complex conjugation, and therefore requires careful handling of the real and imaginary parts of $\tilde{\rho}[\mathbf{n}]$. On the other hand, Eq. (11) indicates a potentially-powerful linear prediction relationship between data measured from opposing sides of the Fourier domain.

Similar to the construction of **C**, Eq. (11) can be transformed into a matrix equation of the form

$$\mathbf{S}\mathbf{h} \approx 0, \tag{12}$$

[§]Our previous work[28] presented two separate low-rank matrix constructions (the **S**- and **G**-matrices) for images with slowly-varying phase. Due to space constraints, we only describe **S**, which has proven more useful in empirical studies.

Downloaded From: http://proceedings.spiedigitallibrary.org/ on 11/21/2016 Terms of Use: http://spiedigitallibrary.org/ss/termsofuse.aspx

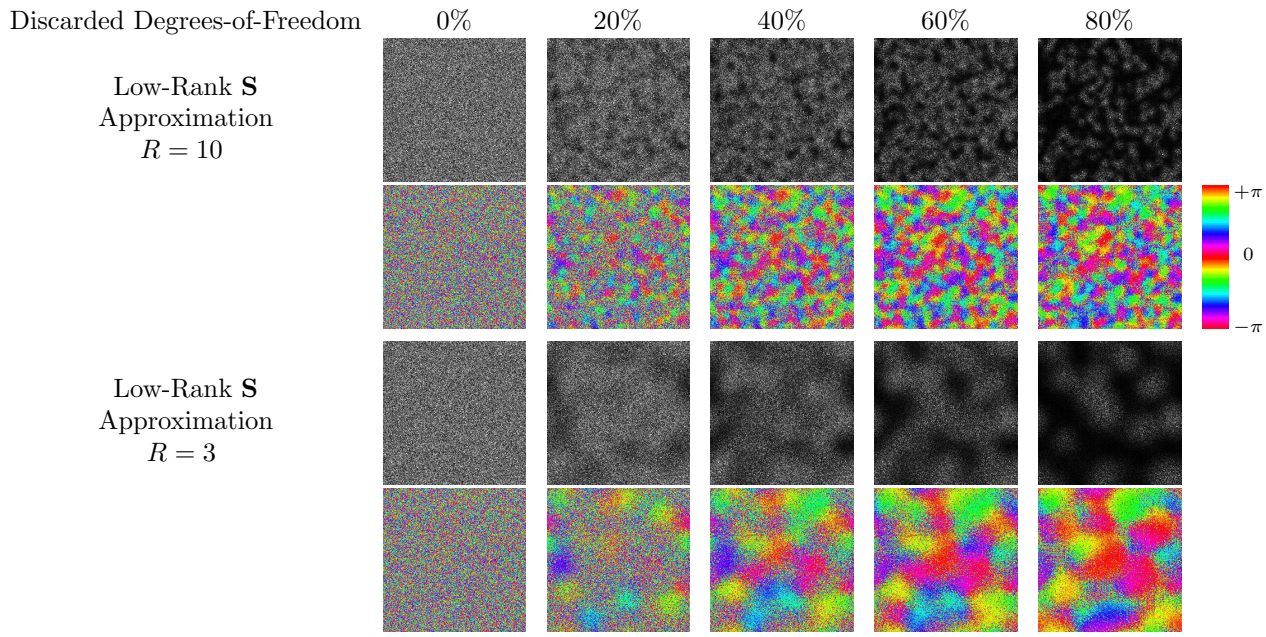

Figure 3: **S**-based low-rank approximation for an image that has neither limited spatial support nor smooth phase. Magnitude (grayscale) and phase (color) images are both shown. Low-rank approximation can impose smooth phase as well as a form of structured (regional) sparsity on the image.

where $\mathbf{S} \in \mathbb{R}^{2Q \times 2|\Lambda|}$ is formed from the real and imaginary components of $\tilde{\rho}[\mathbf{n}]$, and $\mathbf{h} \in \mathbb{R}^{2|\Lambda|}$ is formed from the real and imaginary components of $\tilde{h}[\mathbf{n}]$. Due to space constraints, interested readers should refer to our previous work for details.[28] And similar to the **C** matrix, the **S** matrix will be a low-rank matrix under appropriate assumptions. Specifically, **S** will be low-rank if $\rho(\mathbf{x})$ has smoothly-varying phase and/or has limited spatial support (the image phase is not uniquely defined outside of Ω, which increases the dimension of the nullspace).

For an image that has neither limited spatial support nor smooth phase, low-rank approximation of the **S** matrix has the combined effect of smoothing the image phase and reducing the image support. And, just as with the **C**-matrix, low-rank approximation of **S** imposes these constraints in a structured way, where the spatial scale of the structure depends on the parameter R. This is illustrated in Fig. 3. Note that the phase images in Fig. 3 have been shown using a colorscale that is invariant to π-jumps in the phase, and that if we had shown the phase with it's true periodicity of 2π, then the image phase would not look very smooth. This occurs because conjugate symmetry of the Fourier transform (as used in Eq. (10)) depends on the signal being real-valued, and realness is invariant to π-jumps.

3.3 LORAKS-based Reconstruction

The previous sections described the construction of low-rank matrices **C** and **S** from Nyquist-sampled k-space data. However, in accelerated MRI, Nyquist-sampled k-space data is not available, such that the corresponding **C** and **S** matrices cannot be directly computed. However, the fact that the Nyquist-sampled **C** and **S** matrices should have simple low-rank structure implies that matrix rank constraints could be used to regularize the ill-posed and underdetermined problem of estimating $\tilde{\rho}[\mathbf{n}]$ from undersampled data. This strategy was used in our previous LORAKS work, and often allowed us to obtain high-quality reconstructions of $\tilde{\rho}[\mathbf{n}]$.

Specifically, the LORAKS optimization problem was originally posed as

$$\hat{\tilde{\boldsymbol{\rho}}} = \arg\min_{\tilde{\boldsymbol{\rho}}} \underbrace{\|\mathbf{U}\tilde{\boldsymbol{\rho}} - \mathbf{d}\|_{\ell_2}^2}_{\text{Data Consistency}} + \underbrace{J_C(\mathbf{C}(\tilde{\boldsymbol{\rho}})) + J_S(\mathbf{S}(\tilde{\boldsymbol{\rho}}))}_{\text{Low-Rank Regularization}}, \tag{13}$$

where $\mathbf{C}(\tilde{\boldsymbol{\rho}})$ and $\mathbf{S}(\tilde{\boldsymbol{\rho}})$ are functions of $\tilde{\boldsymbol{\rho}}$ as described previously, and $J_C(\cdot)$ and $J_S(\cdot)$ are regularization penalties that penalize $\mathbf{C}(\tilde{\boldsymbol{\rho}})$ and $\mathbf{S}(\tilde{\boldsymbol{\rho}})$ matrices that have large rank. Regularization penalties that impose low-rank

Downloaded From: http://proceedings.spiedigitallibrary.org/ on 11/21/2016 Terms of Use: http://spiedigitallibrary.org/ss/termsofuse.aspx

matrix structure are becoming increasingly prevalent since the emergence of low-rank matrix recovery theory.[19] While convex low-rank regularization penalties like the nuclear norm[19] are popular in the theoretical literature, non-convex low-rank penalties typically outperform their convex counterparts. Our previous LORAKS results (and all of the new results shown in this paper) are based on the novel non-convex regularization penalties and corresponding algorithms that were introduced in the LORAKS paper.[28] Due to space constraints, we will not describe such details in this paper, though will note one difference from previous LORAKS work: our implementation used an "incremented rank" strategy[44] (with the rank parameters gradually increased during optimization) to make the proposed approach even more resilient to local minima and improve computation speed. Note also that Eq. (13) is easily augmented with additional regularization penalties, meaning that the LORAKS framework is easily combined with other modeling constraints.

3.4 Example LORAKS Reconstruction Results

To illustrate the novel capabilities enabled by the LORAKS framework, this subsection presents some simulated reconstruction results for a range of sampling patterns. These reconstruction results have not appeared in previous literature, though interested readers can find further LORAKS-based simulated- and real-data reconstruction examples in our previous LORAKS publications.[28–33]

The numerical phantom used for simulation is presented in Fig. 4. This phantom has limited spatial support and smoothly varying phase, but the intensity values for each voxel are generated randomly and independently. The randomness of the image magnitude implies that the signal is not very sparse or smooth, and the image has a large rate of innovation. As a result, it would not be very surprising if common sparsity-based image reconstruction methods that impose signal sparsity in the spatial domain ("ℓ_1-Sparsity"[21]) or the finite difference domain ("TV," i.e., total variation[45]) were not very successful. This is confirmed by the results shown in Fig. 5, which show reconstructions derived from several unconventional k-space sampling schemes (in each case, 40% of the full k-space data is measured). Notably, the reconstruction results for LORAKS are much more successful, and LORAKS is the only reconstruction method we are aware of that can be so successful with these nontraditional forms of sampling. Some intuition for the success of LORAKS can be gained from the failure-modes of ℓ_1-Sparsity and TV – in each of these cases, the incorrectly-estimated image support (or, for TV, the transform-domain support) is sparse, but does not possess the geometric structure that realistic images will possess (i.e., there are many isolated non-zero coefficients).[¶] We believe that LORAKS is more successful than these approaches because it prefers images with more realistic structured support and phase characteristics.

4. LORAKS WITH STRUCTURED TRANSFORM-DOMAIN SPARSITY

As originally formulated, the LORAKS matrices $\mathbf{C}$ and $\mathbf{S}$ are formed from the Fourier data of images that have structured sparsity or smooth phase in the image domain. However, in many applications, the images of interest may have better characteristics in a transform domain (e.g., the wavelet domain). For example, most sparsity-based "compressed sensing" methods for MRI have relied on transform-domain sparsity.[20–22] In this section, we note that the LORAKS framework can be modified to impose transform-domain structured sparsity and/or phase constraints. Specifically, let $z(\mathbf{x})$ be a transform-domain representation of $\rho(\mathbf{x})$ that is supported within the FOV and possesses structured sparsity and/or smooth phase, let $\tilde{z}[\mathbf{n}]$ denote the Nyquist-sampled Fourier transform of $z(\mathbf{x})$, and let $\tilde{\mathbf{z}}$ be the vector representation of the fully-sampled $\tilde{z}[\mathbf{n}]$ for some appropriate range of $\mathbf{n}$ values. Then the matrix $\mathbf{C}(\tilde{\mathbf{z}})$ will have low rank. If we assume that the matrix $\mathbf{T}$ is constructed such that $\tilde{\mathbf{z}} = \mathbf{T}\tilde{\boldsymbol{\rho}}$,[‖] then LORAKS can incorporate these transform-domain structured sparsity constraints by replacing (13) with

$$\hat{\tilde{\boldsymbol{\rho}}} = \arg\min_{\tilde{\boldsymbol{\rho}}} \|\mathbf{U}\tilde{\boldsymbol{\rho}} - \mathbf{d}\|_{\ell_2}^2 + J_C(\mathbf{C}(\mathbf{T}\tilde{\boldsymbol{\rho}})) + J_S(\mathbf{S}(\mathbf{T}\tilde{\boldsymbol{\rho}})). \tag{14}$$

This new cost function can be optimized using a small modification of previous LORAKS algorithms.[28]

[¶] Close inspection may be necessary to clearly see the errors in support identification for ℓ_1-Sparsity with Random Checkerboard and Random Partial Fourier sampling.

[‖] The matrix $\mathbf{T}$ will typically transform $\boldsymbol{\rho}$ to the image domain, then transform the resulting image to the sparsity domain, and then apply a Fourier transform to the result.

Downloaded From: http://proceedings.spiedigitallibrary.org/ on 11/21/2016 Terms of Use: http://spiedigitallibrary.org/ss/termsofuse.aspx

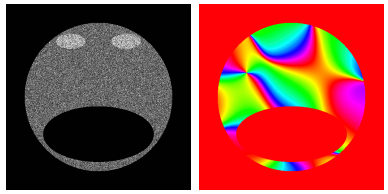

Figure 4: Image used for simulated LORAKS-based reconstruction from undersampled Fourier data. The image magnitude is shown on the left, while the image phase is depicted on the right (same colorscale as Fig. 3).

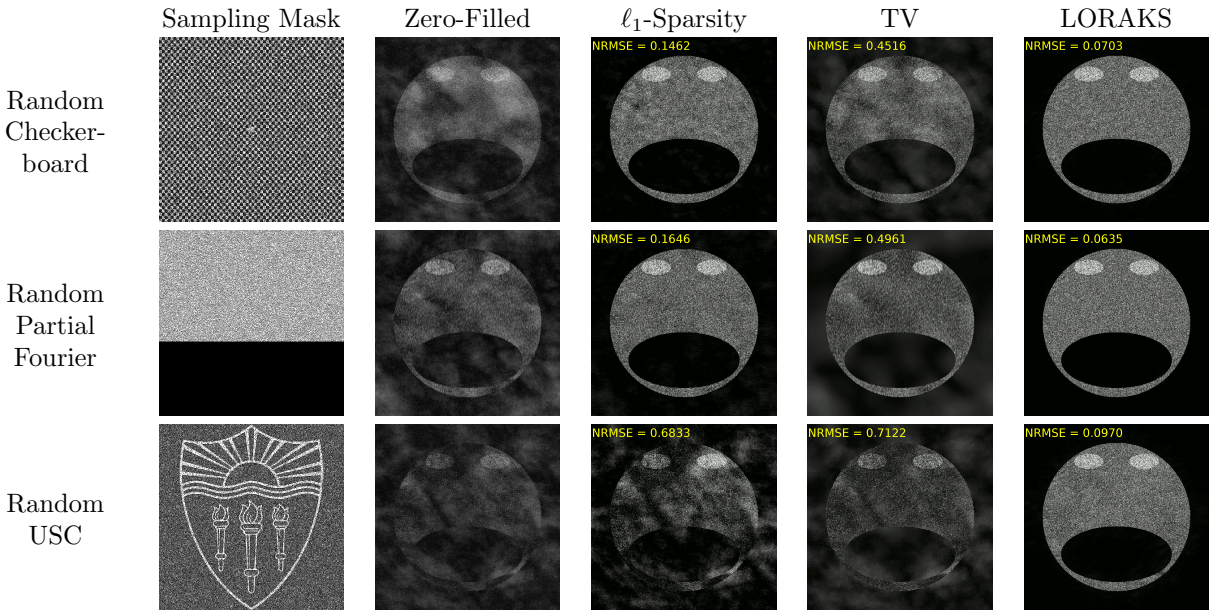

Figure 5: Reconstruction results, with normalized root mean-squared error (NRMSE) values are shown inset. None of these sampling schemes densely samples the center of k-space, which goes against conventional wisdom on MRI compressed sensing sampling design. In addition, the image is not very sparse or smooth. As a result, the failures of ℓ_1-Sparsity and TV are not surprising. However, LORAKS is much more successful.

Using this generalized version of LORAKS requires prior knowledge of an appropriate transform domain (and the corresponding $\mathbf{T}$ matrix). Two examples of promising $\mathbf{T}$ are described in the following subsections, with a comparison given in Section 4.3.

4.1 Piecewise Polynomial Images

Liang *et al.*[11] observed more than 25 years ago that off-the-grid transform-domain sparsity constraints could be imposed on MRI images that possess piecewise polynomial structure. This was achieved by combining low-rank matrix modeling with Fourier-domain representations of spatial differentiation operators, and Liang *et al.* used this idea to enable super-resolution reconstruction from fully-sampled Fourier data. In this work, we note that a suitable $\mathbf{T}$ matrix can be constructed based on the observations of Liang *et al.* to enable these same constraints to be used within the generalized LORAKS framework, therefore enabling a broader class of sampling patterns.

For illustration, consider a 2D scenario with $\rho(\mathbf{x}) = \rho(x, y)$, and let $z(x, y) = \frac{\partial^k}{\partial x^k}\frac{\partial^q}{\partial y^q}\rho(x, y)$ for some choice of integers k and q. If $\rho(x, y)$ is a piecewise polynomial image with polynomial degree bounded by $\max(k, q)$, then the corresponding $z(x, y)$ will vanish everywhere except possibly on the boundaries between the different piecewise polynomial regions. In other words, $z(x, y)$ is sparse, and will possess structured sparsity if the boundaries between different piecewise polynomial regions are well-separated. In addition, the derivative property of the Fourier transform yields that $\tilde{z}[n_x, n_y] = (i2\pi n_x)^k (i2\pi n_y)^q \tilde{\rho}[n_x, n_y]$. This latter relationship implies that a suitable $\mathbf{T}$ matrix can be constructed as a diagonal matrix with diagonal entries equal to the corresponding

Downloaded From: http://proceedings.spiedigitallibrary.org/ on 11/21/2016 Terms of Use: http://spiedigitallibrary.org/ss/termsofuse.aspx

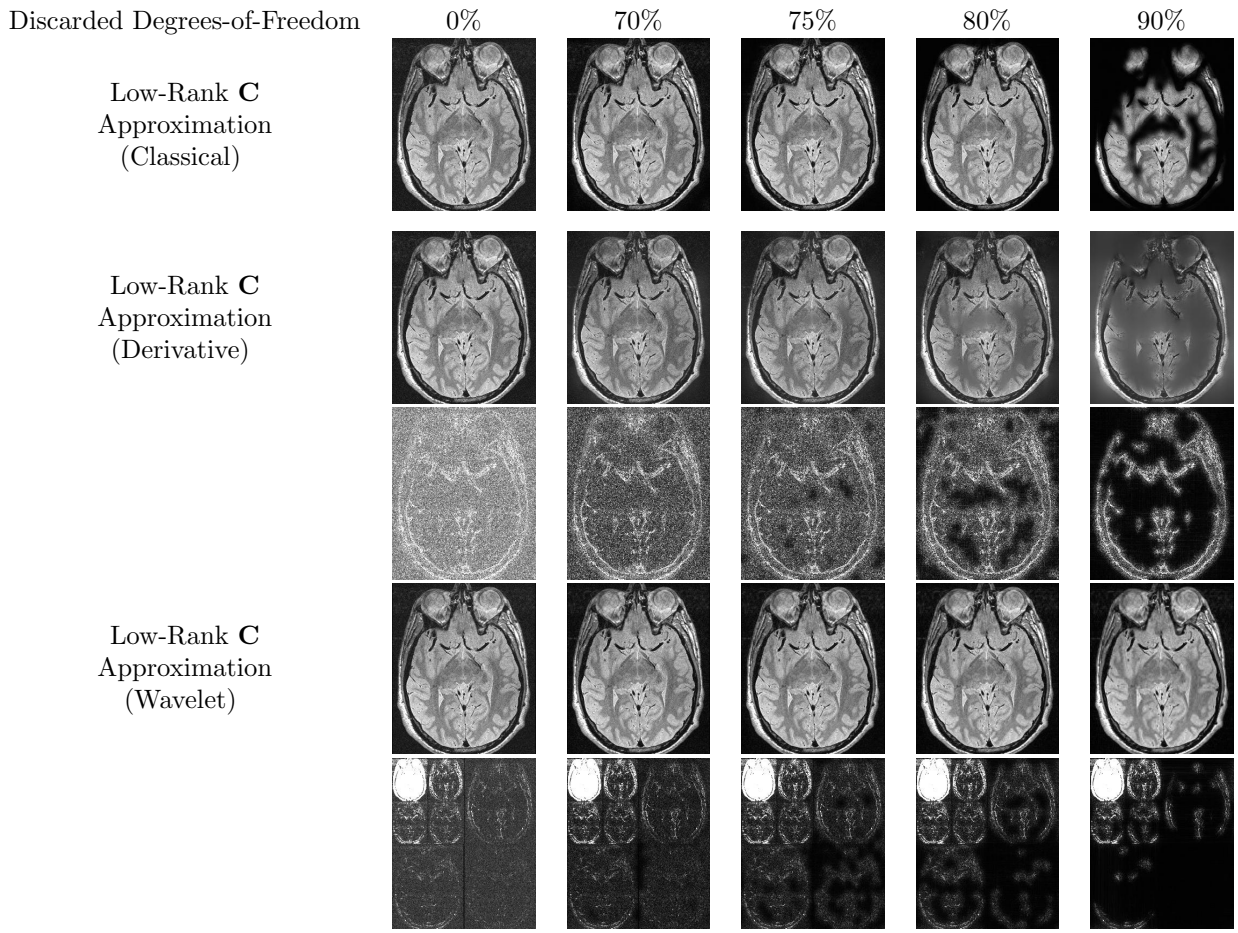

Figure 6: Comparison of different low-rank $\mathbf{C}$ matrix approximations of fully sampled data, with the $\mathbf{C}$ matrix constructed using different transformation matrices $\mathbf{T}$. For (middle) derivitive and (bottom) wavelet sparsity, both the image-domain and transform-domain representations are shown. The two domains coincide for (top) "classical" LORAKS modeling.

$(i2\pi n_x)^k(i2\pi n_y)^q$ weighting factors. As mentioned previously, LORAKS combined with this choice of $\mathbf{T}$ bears certain similarities to recent independent work,[35–37] though also has substantial differences.

4.2 Wavelet Sparsity

Wavelet-domain sparsity constraints are widely used in sparsity-based MRI reconstruction,[20–22] and it is additionally well-known that the wavelet-domain support of a natural image will generally have structured sparsity (with spatial correlation, as well as correlation across different scales and orientations[46]). This wavelet structure lends itself naturally to the structured sparsity constraints that can be imposed using LORAKS. For this paper, we consider a transform matrix $\mathbf{T}$ that is constructed according to $\mathbf{T} = \mathbf{FWF}^{-1}$, where $\mathbf{F}$ is a discrete Fourier transform matrix, and $\mathbf{W}$ implements a wavelet transform. There are many different possible choices of how the wavelet coefficients could be tiled to emphasize different inter- and intra-scale correlation relationships in the support pattern.

4.3 Comparisons

Figure 6 shows a comparison of applying "classical" LORAKS modeling ($\mathbf{T}$ is an identity matrix) against first-order derivative sparsity as described in Section 4.1 ($\mathbf{T}$ is a diagonal matrix with diagonal entries proportional to $\|\mathbf{n}\|_{\ell_1}$) and wavelet-domain sparsity as described in Section 4.2 ($\mathbf{T}$ is formed using an orthogonal Daubechies-4

Downloaded From: http://proceedings.spiedigitallibrary.org/ on 11/21/2016 Terms of Use: http://spiedigitallibrary.org/ss/termsofuse.aspx

wavelet transform matrix $\mathbf{W}$, with wavelet coefficients tiled so that the coefficients from different subbands are spatially separated). In this example, low-rank approximation of the $\mathbf{C}$ matrix** is applied to fully-sampled MRI brain data to illustrate the characteristics and potential benefits of different choices of the $\mathbf{T}$ matrix.

As can be seen, the approximation quality is quite good for each of the different transform domains – image quality is maintained, even with a large number of discarded degrees-of-freedom from the $\mathbf{C}$ matrix. And in each case, sparsity is gradually being imposed in a structured way as the number of discarded degrees-of-freedom increases. For "classical" LORAKS, discarding degrees-of-freedom leads to setting structured regions of the image support equal to zero. Regions with the lowest signal intensity are eliminated first. Similarly, as the number of discarded degrees-of-freedom increases for derivative-based LORAKS, individual regions of the image are gradually set to be piecewise constant. Note that low-rank approximation for this case is quite different than what would be achieved by TV regularization – the LORAKS constraint only imposes that certain regions of the image should be smooth, while other regions of the image are free to still be arbitrarily non-smooth. Wavelet-based LORAKS has similar characteristics – spatially-localized regions from the wavelet domain are gradually being set to zero based on their signal energy, leading to a slow loss of resolution as the number of discarded degrees-of-freedom grows large. For this particular dataset, the "classical" LORAKS and wavelet-based LORAKS variations may be preferable (more parsimonious, leading to better approximation quality and therefore better constrained reconstruction from undersampled data) to derivative-based LORAKS. However, it should be kept in mind that different constraints may be more or less valuable for preserving the image features that are most important for different biomedical MRI application contexts. In addition, since LORAKS constraints are imposed using regularization, it is conceivable to combine multiple different transform-domain LORAKS constraints simultaneously if so desired.

5. DISCUSSION AND CONCLUSIONS

This paper reviewed the LORAKS framework, and presented generalizations of LORAKS for cases where the MR image possesses transform-domain sparsity. The LORAKS framework is quite powerful for imposing phase constraints and/or structured and "off-the-grid" sparsity constraints. Structured sparsity constraints can be substantially more powerful than traditional sparsity, and our empirical results[28–33] suggest that LORAKS can enable novel data sampling strategies that are not very compatible with more conventional sparsity-based image reconstruction approaches. Our results also provide what we believe are new insights into the effects of low-rank matrix approximations on widely-used Toeplitz and Hankel matrices – low-rank matrix approximation of these matrices imposes structured sparsity constraints in a corresponding Fourier transform domain.

The description of LORAKS presented in this paper assumed a very simple MRI data acquisition model, and it should be noted that some of our recent work has considerably widened the practical applicability of the LORAKS framework to realistic MRI problems. For example, P-LORAKS[29] extends LORAKS to the context of multi-channel data acquisition[††], while SMS-LORAKS[32] extends LORAKS and P-LORAKS to the context of simultaneous multislice imaging. In addition, the recent Autocalibrated LORAKS[33] describes a much simpler computationally-inexpensive approach to reconstructing MRI images within the LORAKS framework, which is enabled by the ability to pre-estimate the nullspaces of $\mathbf{C}$ and $\mathbf{S}$ when the k-space data is sampled in a specific "calibration-based" manner.[‡‡] We do not have space to describe these extensions in detail, but refer interested readers to the corresponding references. It should also be noted that while LORAKS was developed within the context of MRI, we believe that the ideas and methods generalize naturally to a variety of other signal processing and inverse problem contexts where structured sparsity and/or slowly-varying phase are meaningful constraints.

ACKNOWLEDGMENTS

This work was supported in part by NSF CAREER award CCF-1350563 and NIH grant R01-NS074980.

**This data was acquired with a 4-channel array of receiver coils, so we use the multichannel construction of the $\mathbf{C}$ matrix described in our recent P-LORAKS work[29] instead of the single-channel construction described in this paper.

††$\mathbf{C}$-based P-LORAKS has strong similarities to the earlier SAKÉ method,[26] though P-LORAKS has more flexibility and distinct advantages.

‡‡Special cases of the Autocalibrated LORAKS framework also have strong similarities to certain existing methods,[8,47] though Autocalibrated LORAKS again has more flexibility and distinct advantages.

Downloaded From: http://proceedings.spiedigitallibrary.org/ on 11/21/2016 Terms of Use: http://spiedigitallibrary.org/ss/termsofuse.aspx

REFERENCES

[1] Liang, Z.-P., Boada, F., Constable, T., Haacke, E. M., Lauterbur, P. C., and Smith, M. R., "Constrained reconstruction methods in MR imaging," *Rev. Magn. Reson. Med.* **4**, 67–185 (1992).

[2] Plevritis, S. K. and Macovski, A., "Spectral extrapolation of spatially bounded images," *IEEE Trans. Med. Imag.* **14**, 487–497 (1995).

[3] Xiang, Q.-S. and Henkelman, R. M., "K-space description for MR imaging of dynamic objects," *Magn. Reson. Med.* **29**, 422–428 (1993).

[4] Madore, B., Glover, G. H., and Pelc, N. J., "Unaliasing by Fourier-encoding the overlaps using the temporal dimension (UNFOLD), applied to cardiac imaging and fMRI," *Magn. Reson. Med.* **42**, 813–828 (1999).

[5] Tsao, J., Boesiger, P., and Pruessmann, K. P., "k-t BLAST and k-t SENSE: Dynamic MRI with high frame rate exploiting spatiotemporal correlations," *Magn. Reson. Med.* **50**, 1031–1042 (2003).

[6] Margosian, P., Schmitt, F., and Purdy, D., "Faster MR imaging: imaging with half the data," *Health Care Instrum.* **1**, 195–197 (1986).

[7] Noll, D. C., Nishimura, D. G., and Macovski, A., "Homodyne detection in magnetic resonance imaging," *IEEE Trans. Med. Imag.* **10**, 154–163 (1991).

[8] Huang, F., Lin, W., and Li, Y., "Partial Fourier reconstruction through data fitting and convolution in k-space," *Magn. Reson. Med.* **62**, 1261–1269 (2009).

[9] Hu, X., Levin, D. N., Lauterbur, P. C., and Spraggins, T., "SLIM: Spectral localization by imaging," *Magn. Reson. Med.* **8**, 314–322 (1988).

[10] Haacke, E. M., Liang, Z.-P., and Izen, S. H., "Superresolution reconstruction through object modeling and parameter estimation," *IEEE Trans. Acoust., Speech, Signal Process.* **37**, 592–595 (1989).

[11] Liang, Z.-P., Haacke, E. M., and Thomas, C. W., "High-resolution inversion of finite Fourier transform data through a localised polynomial approximation," *Inverse Probl.* **5**, 831–847 (1989).

[12] Hu, X., Johnson, V., Wong, W. H., and Chen, C.-T., "Bayesian image processing in magnetic resonance imaging," *Magn. Reson. Imag.* **9**, 611–620 (1991).

[13] Smith, M. R., Nichols, S. T., Henkelman, R. M., and Wood, M. L., "Application of autoregressive moving average parametric modeling in magnetic resonance image reconstruction," *IEEE Trans. Med. Imag.* **MI-5**, 132–139 (1986).

[14] Barone, P. and Sebastiani, G., "A new method of magnetic resonance image reconstruction with short acquisition time and truncation artifact reduction," *IEEE Trans. Med. Imag.* **11**, 250–259 (1992).

[15] Martin, J. F. and Tirendi, C. F., "Modified linear prediction modeling in magnetic resonance imaging," *J. Magn. Reson.* **82**, 392–399 (1989).

[16] Hess, C. P. and Liang, Z.-P., "A data-consistent linear prediction method for image reconstruction from finite Fourier samples," *Int. J. Imag. Syst. Tech.* **7**, 136–140 (1996).

[17] Donoho, D. L., "Compressed sensing," *IEEE Trans. Inf. Theory* **52**, 1289–1306 (2006).

[18] Candès, E. and Tao, T., "Near optimal signal recovery from random projections: Universal encoding strategies," *IEEE Trans. Inf. Theory* **52**, 5406–5425 (2006).

[19] Recht, B., Fazel, M., and Parrilo, P. A., "Guaranteed minimum-rank solutions of linear matrix equations via nuclear norm minimization," *SIAM Rev.* **52**, 471–501 (2010).

[20] Haldar, J. P., Hernando, D., and Liang, Z.-P., "Compressed-sensing MRI with random encoding," *IEEE Trans. Med. Imag.* **30**, 893–903 (2011).

[21] Lustig, M., Donoho, D., and Pauly, J. M., "Sparse MRI: The application of compressed sensing for rapid MR imaging," *Magn. Reson. Med.* **58**, 1182–1195 (2007).

[22] Trzasko, J. and Manduca, A., "Highly undersampled magnetic resonance image reconstruction via homotopic ℓ_0-minimization," *IEEE Trans. Med. Imag.* **28**, 106–121 (2009).

[23] Jung, H., Sung, K., Nayak, K. S., Kim, E. Y., and Ye, J. C., "k-t FOCUSS: A general compressed sensing framework for high resolution dynamic MRI," *Magn. Reson. Med.* **61**, 103–116 (2009).

[24] Haldar, J. P. and Liang, Z.-P., "Spatiotemporal imaging with partially separable functions: A matrix recovery approach," in [*Proc. IEEE Int. Symp. Biomed. Imag.*], 716–719 (2010).

Downloaded From: http://proceedings.spiedigitallibrary.org/ on 11/21/2016 Terms of Use: http://spiedigitallibrary.org/ss/termsofuse.aspx

[25] Lingala, S. G., Hu, Y., DiBella, E., and Jacob, M., "Accelerated dynamic MRI exploiting sparsity and low-rank structure: k-t SLR," *IEEE Trans. Med. Imag.* **30**, 1042–1054 (2011).

[26] Shin, P. J., Larson, P. E. Z., Ohliger, M. A., Elad, M., Pauly, J. M., Vigneron, D. B., and Lustig, M., "Calibrationless parallel imaging reconstruction based on structured low-rank matrix completion," *Magn. Reson. Med.* **72**, 959–970 (2014).

[27] Trzasko, J. D. and Manduca, A., "CLEAR: Calibration-free parallel imaging using locally low-rank encouraging reconstruction," in [*Proc. Int. Soc. Magn. Reson. Med.*], 517 (2012).

[28] Haldar, J. P., "Low-rank modeling of local k-space neighborhoods (LORAKS) for constrained MRI," *IEEE Trans. Med. Imag.* **33**, 668–681 (2014).

[29] Haldar, J. P. and Zhuo, J., "P-LORAKS: Low-rank modeling of local k-space neighborhoods with parallel imaging data," *Magn. Reson. Med.* (2015). In Press.

[30] Haldar, J. P., "Calibrationless partial Fourier reconstruction of MR images with slowly-varying phase: A rank-deficient matrix recovery approach," in [*Proc. ISMRM Workshop on Data Sampling & Image Reconstruction*], (2013).

[31] Haldar, J. P., "Low-rank modeling of local k-space neighborhoods (LORAKS): Implementation and examples for reproducible research," Tech. Rep. USC-SIPI-414, University of Southern California, Los Angeles, CA (April 2014).

[32] Kim, T. H. and Haldar, J. P., "SMS-LORAKS: Calibrationless simultaneous multislice MRI using low-rank matrix modeling," in [*Proc. IEEE Int. Symp. Biomed. Imag.*], 323–326 (2015).

[33] Haldar, J. P., "Autocalibrated LORAKS for fast constrained MRI reconstruction," in [*Proc. IEEE Int. Symp. Biomed. Imag.*], 910–913 (2015).

[34] Cheung, K. F. and Marks II, R. J., "Imaging sampling below the Nyquist density without aliasing," *J. Opt. Soc. Am. A* **7**, 92–105 (1990).

[35] Ongie, G. and Jacob, M., "Super-resolution MRI using finite rate of innovation curves," in [*Proc. IEEE Int. Symp. Biomed. Imag.*], (2015). In Press.

[36] Ongie, G. and Jacob, M., "Recovery of piecewise smooth images from few Fourier samples," in [*SampTA*], (2015).

[37] Jin, K. H., Lee, D., and Ye, J. C., "A novel k-space annihilating filter method for unification between compressed sensing and parallel MRI," in [*Proc. IEEE Int. Symp. Biomed. Imag.*], (2015). In Press.

[38] Blu, T., Dragotti, P.-L., Vetterli, M., Marziliano, P., and Coulot, L., "Sparse sampling of signal innovations: Theory, algorithms, and performance bounds," *IEEE Signal Process. Mag.* **25**, 31–40 (2008).

[39] Chen, Y. and Chi, Y., "Robust spectral compressed sensing via structured matrix completion," *IEEE Trans. Inf. Theory* **60**, 6576–6601 (2014).

[40] Gürelli, M. İ. and Nikias, C. L., "EVAM: An eigenvector-based algorithm for multichannel blind deconvolution of input colored signals," *IEEE Trans. Signal Process.* **43**, 134–149 (1995).

[41] Xu, G., Liu, H., Tong, L., and Kailath, T., "A least-squares approach to blind channel identification," *IEEE Trans. Signal Process.* **43**, 2982–2993 (1995).

[42] Harikumar, G. and Bresler, Y., "Blind restoration of images blurred by multiple filters: theory and efficient algorithms," *IEEE Trans. Image Process.* **8**, 202–219 (1999).

[43] Tang, G., Bhaskar, B. N., Shah, P., and Recht, B., "Compressed sensing off the grid," *IEEE Trans. Inf. Theory* **59**, 7465–7490 (2013).

[44] Haldar, J. P. and Hernando, D., "Rank-constrained solutions to linear matrix equations using PowerFactorization," *IEEE Signal Process. Lett.* **16**, 584–587 (2009).

[45] Rudin, L. I., Osher, S., and Fatemi, E., "Nonlinear total variation based noise removal algorithms," *Physica D* **60**, 259–268 (1992).

[46] Simoncelli, E. P., "Statistical models for images: Compression, restoration and synthesis," in [*Proc. Asilomar Conf. on Signals, Systems, and Computers*], 673–678 (1997).

[47] Zhang, J., Liu, C., and Moseley, M. E., "Parallel reconstruction using null operations," *Magn. Reson. Med.* **66**, 1241–1253 (2011).

Downloaded From: http://proceedings.spiedigitallibrary.org/ on 11/21/2016 Terms of Use: http://spiedigitallibrary.org/ss/termsofuse.aspx